THE JOURNAL OF PHYSICAL CHEMISTRY B

Article

pubs.acs.org/JPCB

Arrangement of Fibril Side Chains Studied by Molecular Dynamics and Simulated Infrared and Vibrational Circular Dichroism Spectra

Jiří Kessler,[†,‡] Timothy A. Keiderling,*[,§] and Petr Bouř*[,†]

[†]Institute of Organic Chemistry and Biochemistry, Academy of Sciences, Flemingovo náměstí 2, 166 10 Prague, Czech Republic

[‡]Department of Physical and Macromolecular Chemistry, Faculty of Science, Charles University, Hlavova 8, 128 40 Prague, Czech Republic

[§]Department of Chemistry, University of Illinois at Chicago, 845 West Taylor Street, Chicago, Illinois 60607-7061, United States

Supporting Information

ABSTRACT: Highly ordered assemblies of β-sheet-forming peptide and protein fibrils have been the focus of much attention because of their multiple and partially unknown biological functions, in particular as related to degenerative neuronal disorders. Recently, vibrational circular dichroism (VCD) spectra have been shown to provide a unique means of detection for such extended structures utilizing modes of the peptide main chain backbone. In the case of poly-glutamic acid, surprising VCD responses were also found for side chain modes. In this study, in an attempt to explain this latter observation and obtain a link between fibrillar structure and its optical spectral properties, molecular dynamics (MD) methods are used to model the geometry and dynamics of assemblies containing repeating β-strands of Glu_n. A crystal-like model was adopted for the MD structure simulations. Infrared and VCD spectra for segments of MD modeled fibrillar geometries were first calculated using density functional theory (DFT), and then, those parameters were applied to larger structures by means of Cartesian coordinate transfer (CCT) of atomic tensors from the segments. The computations suggest the side chains exhibit residual conformational constraints, resulting in local coupling giving rise to non-negligible VCD intensity, albeit with an overall broad distribution. Calculated spectral distributions are qualitatively consistent with the experimental results but do differ in magnitude. The possibility of realistic modeling of vibrational spectra significantly broadens the potential for application of optical spectroscopies in structural studies of these aggregated biopolymers.

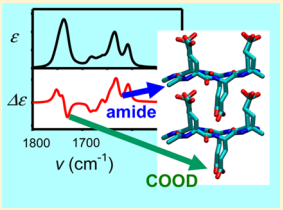

INTRODUCTION

Structure and interactions of fibrils and similar protein aggregates are intensively studied because of the appearance of that morphology for many proteins and peptides associated with the symptoms of several neurodegenerative diseases (Alzheimer's, Parkinson's, Huntington's, etc.).[1] More fundamentally, such structures are of interest due to the general need to understand alternate aspects of peptide and protein folding (or mis-folding) and the associated molecular interactions that drive such structure formation.[2] However, insight into the structure and other physical properties of fibrils remains rather limited. For example, structural irregularities in solid phase samples can make conventional X-ray studies and thus spatial resolution at the atomic level impossible.[3] At the same time, difficulties in solubilizing such fibrils to a uniform distribution can cause difficulties for some spectroscopic studies, preventing reliable analyses.[4−8]

In spite of these problems, electronic[9] and vibrational spectra,[10] in particular coupled with circular dichroism (CD), have revealed unique properties of fibrillar structures. Traditional tests of fibril formation have involved fluorescence changes of adsorbed dyes, such as thioflavin T, and detection of induced CD in the ultraviolet (UV). More recently, vibrational circular dichroism (VCD, the differential absorption of left- and right-circularly polarized light in the infrared, IR) has been shown to detect the sense of supermolecular fibrillar twist and some degree of fibrillar assembly (and even morphology, e.g., thin ribbons vs helical aggregates), as confirmed by complementary atomic force microscopy (AFM) studies.[10−18] Such vibrational spectra can be computationally modeled, even for relatively large structures, permitting development of structure−spectra correlations on a fundamental level.[19−23]

In principle, the structural basis of such spectral responses can be obtained via quantum chemical simulations. However, large size molecules and molecular aggregates pose a challenge due to the nonlinear scaling of more reliable calculations that use, for example, density functional theory (DFT) methods. If the structures are regular, it is possible to compute spectral properties of a limited number of fragments and transfer those onto a larger structure. We have shown this method to work well for computations of vibrational spectra, particularly IR and VCD by use of a Cartesian coordinate transfer method (CCT).[24−26] The complexity of an aggregated peptide structure makes complete understanding and simulations of all spectral features rather difficult. The resultant spectral bandshapes and frequency distributions are dependent on both local conformation of the peptide chains (secondary structure)[27] and longer-range coupling through periodic

Received: March 3, 2014
Revised: May 22, 2014
Published: May 28, 2014

   dx.doi.org/10.1021/jp502178d | J. Phys. Chem. B 2014, 118, 6937−6945

structures enabling vibrational mode delocalization.[28] With formation of supermolecular structure, these polymeric interactions gain another dimension, becoming coherent (ordered) in a relatively large particle, which can alter the intensities of various underlying spectral components. Vibrational spectra, including IR and VCD intensities, can be reliably calculated with relatively efficient DFT computations for peptides of moderate size.[29,30] These computations can be extended to larger molecular assemblies with the CCT method, provided reasonable structures can be determined.[24−26] In this way, spectra of structures containing extended single or multiple sheets (each with many strands) can be simulated and related to experimental data.[31−33]

Poly-L-glutamic acid at low pH has low solubility and upon heating forms an aggregate with an underlying β-sheet secondary structure that has unusual characteristics, which are evidenced as a higher density structure correlated to a decrease in intersheet separation and an IR spectrum having an amide I (primarily C═O stretch) band with a maximum below 1600 cm^{-1}, which is much lower than normal for β-sheets. This has been termed a β_2 structure, whose unique low-frequency amide I character (<1600 cm^{-1}) and prominent (~1730 cm^{-1}) —COOD stretching band has been attributed to bifurcated H-bonding of the amide C═O both intrasheet, i.e., cross-strand to other amide N—H groups, and intersheet to side-chain carboxylic acid, —COOH, groups associated with a neighboring (stacked) sheet.[4,34,35] The VCD spectrum correlates to this IR pattern with an intense couplet shape centered on the most intense, lower frequency amide I IR component and a weaker couplet (or sometimes three-band pattern) associated with the —COOH side chain band.[4,36]

Simulating spectra for such poly-glutamic acid[4] structures poses new challenges. While spectra of both the side chain and backbone indicate ordering, the degree of order is probably not the same. Normally, side-chain modes result in zero or very weak VCD, in that the VCD spectrum of an otherwise achiral side-chain chromophore (e.g., −COOH) must arise primarily from through-space coupling or a systematic geometry perturbation coming from at least partially ordered repeating structures. Because of the significant conformational freedom of such side chains, modeling the fibril structure based on a complete conformer search is not reasonable.

Therefore, as a first approximation to the fibrillar structure, we used molecular dynamics (MD) techniques to simulate the dense fibril-like structure with highly ordered strands, and explored initial effects of backbone and side chain flexibility using pseudocrystal-like periodic boundary conditions. Once a stable assembly was established, snapshots of structures along the trajectory were used as a basis for DFT computations of IR and VCD spectral parameters for fragments of the sheet structures that contain several interacting amide and carboxylic acid groups. The CCT method was then adopted to transfer these DFT spectral parameters from fragment computations to effectively model spectra of quite large segments of fibril structures. The variations in structures obtained were then encompassed in our spectral simulations by obtaining an average for a sufficient number of structures derived from MD trajectory snapshots. The results show that, even for largely disordered fibril side chains, a net −COOH (or −COOD) VCD can develop, qualitatively reflecting some underlying order in the side chains leading to their coupling. While these results do not fit all the experimental details, they do suggest an origin for observed Glu_n IR and VCD results and demonstrate that a combined quantum chemical/MD simulation can provide a link between formation of supermolecular structure and its spectroscopic response.

METHODS

Molecular Dynamics. For two 15-amide protonated poly-glutamic acid (PLGA) strands, $[Ac\text{-}Glu_{14}\text{-}NH_2]_2$, with acetyl on the N-terminus and $-NH_2$ on the C-terminus as in Figure 1,

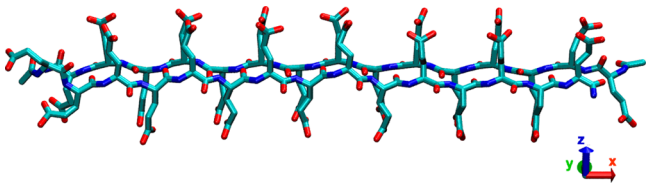

Figure 1. Two peptide strands ($[Ac\text{-}(Glu)_{15}\text{-}CONH_2]_2$) placed in antiparallel arrangement into the periodic box; hydrogen atoms and 15 water molecules terminating the box in the *x*-direction are not shown. This snapshot structure results after annealing the initial more twisted structure taken from experiment (see Figure S1, Supporting Information) under constraint of periodic boundary conditions.

the initial geometry (see Figure S1 in the Supporting Information) structure was placed in a monoclinic periodic box (66.00 Å × 9.77 Å × 8.07 Å, α = 105°). The remaining space in the *x*-direction was filled with 15 water molecules, with no waters coming between strands or sheets (i.e., unit cells in *y*- and *z*-direction). The initial geometry was based on an analysis of a previously published X-ray pattern of poly-L-glutamic acid (PLGA) powder (Figure S1, Supporting Information).[34,35] Using the Gromacs program[37] and Amber03 force field,[38] the system was equilibrated as an *NVT* ensemble by simulated annealing, from 1000 to 300 K. For the *NVT* ensemble, 19 independent annealing cycles were performed, with times ranging from 0.7 to 1.6 ns, to achieve the randomization. Each annealing was followed by a 10 ns equilibration and 100 ns production stage, at this stage with both with *NpT* and *NVT* conditions, using T = 300 K and p = 1 atm. For the *NpT* dynamics, the final box dimensions stabilized at geometries close to the X-ray geometry, with an average dimension (with RMS deviations) of 66.15 (0.19) Å × 9.79 (0.03) Å × 8.09 (0.02) Å.

Spectral Generation. To better represent important vibrational interactions within and between the β-sheet planes and to minimize end-effects, aggregate sheet structures were created for spectral modeling from multiple representations of the periodic box or unit cell (Figure 1). The assembly was expanded in the sheet stacking interaction direction, or *z*-direction, creating stacks of two or four two-stranded antiparallel sheets (e.g., systems "**z2**" and "**z4**"), and also in the *y*-direction (interstrand H-bonded direction) to allow consideration of larger, four-stranded sheets (providing systems as "**y2z2**" and "**y2z3**"). The largest **y2z3** assembly is composed of three four-stranded antiparallel sheets, stacked with the same (in-phase) relative alignment, and was used for the final spectral generation, while smaller structures were used for various tests.

Absorption and VCD spectra of these model systems were obtained by computing harmonic force field and atomic polar and axial tensor parameters for smaller fragments. The fragments comprised 8- and 12-amide-containing molecules (illustrated as the **F8** and **F12** structures in Figure 2). By default, the more extended **F12** model was used to provide a

dx.doi.org/10.1021/jp502178d | J. Phys. Chem. B 2014, 118, 6937−6945

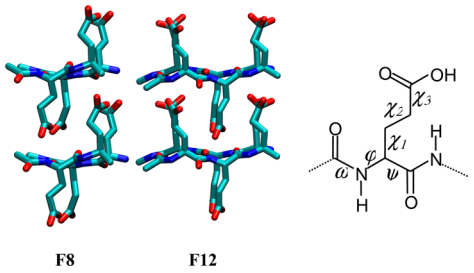

Figure 2. (left) Fragments [Ac-Glu-CONH-CH($CH_2CH_2CO_2H$)-Me·NH_2-Glu_2-CONHMe]$_2$ (**F8**) and [Ac-Glu_2-CONH-CH-($CH_2CH_2CO_2H$)-Me·NH_2-Glu_3-CONHMe]$_2$ (**F12**) used in the DFT computations and (right) principle torsion angles in the Glu residue.

comparison to experiment, whereas the smaller **F8** system enabled us to shorten the computational time and perform additional convergence and other theoretical tests, which are discussed at the end of the following section. To represent the variety of side chain conformations present in the MD runs, 16/24 (for **F8**/**F12**, respectively) fragment conformations were derived from four randomly chosen MD snapshots captured along one trajectory, separated by about 15 ns, both for the *NpT* and *NVT* conditions. Then, fragments had a variety of side-chain conformations and came from both the middle of the sequence and segments adjacent to but not on the termini.

The fragments were then partially geometry optimized in normal mode coordinates.[39−41] By constraining motion along normal coordinates whose modes had frequencies below 300 cm^{-1}, the MD geometry distribution could be largely conserved, while the higher energy coordinates important for the spectra (e.g., C═O stretching) could be completely relaxed. The Gaussian program[42] and the BPW91[43]/6-31G** level of approximation were used. The crystal/fibril environment was simulated using the COSMO dielectric solvent model[44] with a water dielectric constant (ε_r = 78), presumably close to that of the aggregated peptide. Although it is known that the BPW91 functional slightly underestimates harmonic vibrational frequencies,[45] it provides a reasonable and efficient basis for simulation of vibrational properties of the amide and carboxyl groups including their VCD spectra.[33]

The force field and tensors were calculated with the Gaussian programs and transferred[24−26] to the target sheet assemblies (**z2**, **z4**, **y2z2**, **y2z3**) selected for spectral modeling. To complete the transfer, parameters for each atom pair in the three target structures were selected on the basis of determining the best overlap obtained with the corresponding atoms in each of the 16 or 24 fragments (depending on the model, **F8** or **F12**, used). The RMS distance between the closest covalently bound atoms was taken as the criterion for overlap quality. For the assemblies, absorption and VCD spectral frequencies and intensities were generated by usual procedures.[46] Lorentzian profiles (10 cm^{-1} full width at half-maximum) were assigned to each mode, scaled to its intensity, and summed to obtain overall IR (ε) and VCD ($\Delta\varepsilon$) band shapes. The calculated intensities are given in the usual units of L mol^{-1} cm^{-1}, normalized to one amino acid residue.

The spectra were simulated for structural snapshots obtained 10 ns apart for trajectories starting from each of the 19 annealed structures. These were then averaged to provide representations of the final computed spectra for both the *NVT* and *NpT* trajectories. Since experiments are predominantly conducted in D_2O, all spectra were computed to represent deuteration (H/D exchange) of the NH and COOH groups.

As an alternative to the *ab initio*, tensor transfer approach, the transition dipole coupling (TDC) model[47,48] was used to generate the absorption and VCD spectra of **y2z2** as a test. The transition electric dipole moments and frequencies of the C═O stretching vibration were calculated for the CH_3CO—$NDCH_3$ and CH_3COOD (separate computations for the *cis*- and *trans*-OD conformation) molecules at the BPW91/6-31G**/COSMO(H_2O) level and transferred to the fibrillar geometry. For amide I simulations, dipoles were placed in the middle of the C═O bonds, and the TDC Hamiltonian comprised only of the dipole−dipole interactions was diagonalized. This procedure does not include the frequency dispersion due to the DFT force field, since all the amide or —COOD oscillators are initially degenerate and the resultant dispersion is only from their dipolar coupling. From the obtained coupled frequencies and intensities, the spectra were generated as described above.

RESULTS AND DISCUSSION

Molecular Dynamics. The *NpT* conditions could not be maintained during the annealing because at computed high temperatures the strands would not remain H-bonded and would effectively "evaporate". Consequently, we computed the 19 *NVT* annealed structures and then ran both *NVT* and *NpT* trajectories starting from those initial structures. The final *NpT* elementary cell size (periodic box) dimensions were very close to the original postulated *NVT* structure of 66.00 × 9.77 × 8.07 $Å^3$ based on the powder X-ray studies.[35] This indicates that the model geometry used as well as the Amber03 force field might be realistic for PLGA fibrils.

Our postulated conformation corresponds to the β_2 form of PLGA which forms fibrillar structures at low pH and higher temperatures.[4,35,49] This compact form with an intersheet spacing of 8.07 Å was initially designated as β_2 by Itoh and Fasman[35] to contrast with the more typical β_1 form. For PLGA, the β_1 form diffraction data indicates a larger intersheet spacing of 9.35 Å, and it condenses as a less dense gel from the soluble pH ∼ 4 (α-helical) PLGA solution immediately upon heating. By contrast, the β_2 form requires extended incubation at higher temperatures, and can be further affected in yield by lower pH. These forms are also possible to obtain with Glu oligopeptides, under somewhat different aggregation conditions, and have both been shown to have antiparallel sheet secondary structures with possibly different interstrand registries.[36] The registry was determined by isotopic labeling with Val and is likely to be a function of the substitution sequence used.

In Figure 3, equilibrium distributions for various torsional angles are plotted as averages of 19 annealing cycles (black traces), which are almost identical to those obtained using only 9 annealing cycles (red traces), indicating convergence. Additionally, the *NVT* and *NpT* trajectories result in very similar angular distributions (Figure 3, left and right) with only minor differences. The ω-torsion angle oscillates around the usual value of 180°, and the relatively large amplitude suggests unusual flexibility of the otherwise planar and conjugated π-electron amide system.[50,51] Only the terminal amides had any propensity for the *cis* conformation, resulting in the small population at $\omega \sim 0°$. Average φ and ψ angles (about −160 and 150°, respectively) correspond reasonably well to canonical antiparallel β-sheet values (−139 and 135°).[52] The side chain angles χ_1 and χ_2 also exhibit surprisingly narrow distributions,

dx.doi.org/10.1021/jp502178d | J. Phys. Chem. B 2014, 118, 6937−6945

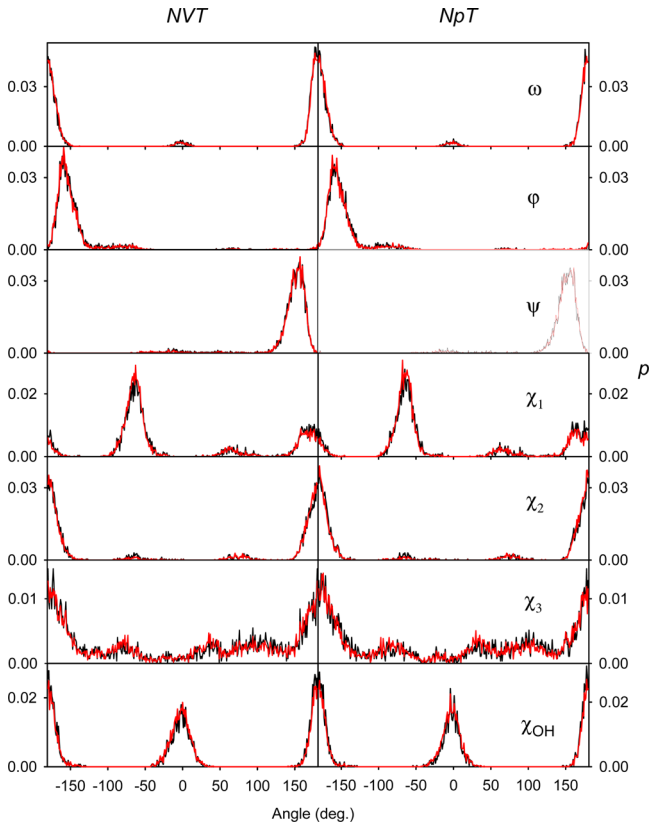

Figure 3. Equilibrium angular distributions calculated for the *NVT* and *NpT* ensembles. The average obtained from 19 annealing cycles is plotted in black, and an intermediate average from 9 cycles is in red.

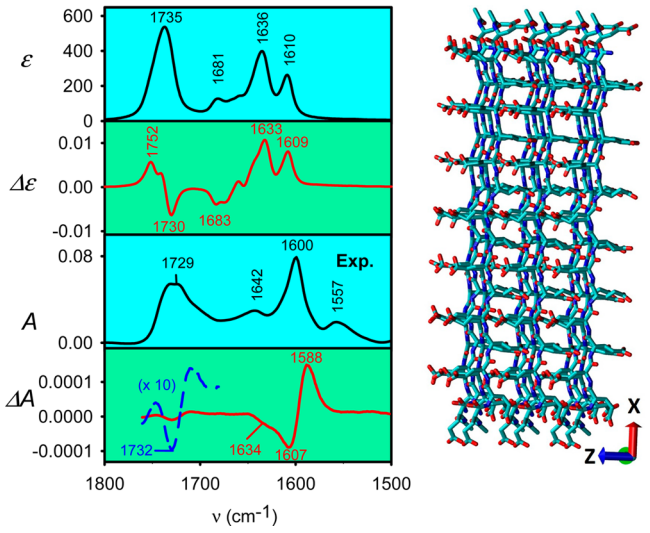

Figure 4. Simulated spectra (*NVT* ensemble) for the **y2z3** fibrillar structure (transfer from **F12**) and experimental spectra for **E10** fibrils formed at pH 1 in DCl/D_2O solvent and room temperature. (For the experimental data, the expanded —COOD part of the VCD spectrum is added as the blue dashed line; the residual experimental absorbance at ~1557 cm^{-1} is probably due to unexchanged amides, i.e., amide II mode; because of difficulties in determining the concentration, absorbance units are used, which suggests comparison is best done on the basis of $\Delta A/A$ values referenced to peak absorbance intensities.) Directions of the Cartesian axis are indicated; *y* and *z* approximately align with the *b* and *c* monoclinic periodic box axes ($\alpha = \angle bc = 105°$).

not much broader than those for φ and ψ, with maxima at about −70 and 180°, respectively, and minor populations for other rotamers (particularly χ_1 at ~70 and ~170°). By contrast, χ_3 apparently can adopt many values but favors an extended conformation ($\chi_3 = 180°$), as indicated by the probability plots. Angle χ_{OH} is again rather constrained, either 0 or 180°, lying in the COO plane, as expected. Although all of the angles strongly prefer one or two positions, the simulations do not indicate that the side chain geometries would adopt a regular crystal-like pattern. At the high temperatures of the annealing (under the *NVT* conditions), the side chains move freely but stay lined up within the gaps provided by the side chains on the opposing sheets, eventually becoming disordered due to χ_3 at the −COOH ends. However, the peptide backbone remains aligned and stacked at T = 300 K for the *NVT* and *NpT* runs, and this common aspect of the structure is maintained in the trajectories.

Comparison of Modeled Spectra to Experiment. The averaged simulated absorption and VCD spectra for the **y2z3** (deuterated) system are plotted in Figure 4, and compared there with the recently published experimental spectra for the Glu_{10} oligopeptide fibrils (**E10**).[36] The **E10** fibril data is given as a typical example; longer poly-glutamic acid chains as well as models with Val or Leu substitutions provide somewhat different experimental VCD spectra that are dependent on conditions of fibril preparation and methods of sampling.[4,36] The IR experimental pattern of PLGA fibrils in various systems is less affected by chain length.[4,49]

In Figure 4, we can see a reasonable correspondence between the observed and simulated IR patterns. The absorption peak calculated at 1735 cm^{-1} and observed at 1729 cm^{-1} corresponds to the C═O stretching vibration of the COOD group (as obtained in D_2O solution). In the experimental spectrum, this peak is slightly split for all Glu sequences but is one band with a lower frequency shoulder for mixed sequences. The splitting is less apparent in the averaged simulated spectrum with the 10 cm^{-1} bandwidth, where only a shoulder is seen. A more detailed analysis (dynamic normal mode displacement) of the simulations suggests that two types of modes contribute to this band, correlated to the *cis* and *trans* orientations of the OD group with respect to the vibrating carbonyl group. The *cis* orientation provides slightly lower frequencies for this vibration, i.e., closer to the amide I region.

The absorption maxima calculated at 1681, 1636 (with a weak feature at ~1670 cm^{-1}), and 1610 cm^{-1} are primarily composed of C═O stretching of the amide groups ("amide I" bands) and may be associated with the experimental maxima evident at 1642 and 1600 cm^{-1}. The computed amide I bands are all higher in frequency than the corresponding experimental values and have a greater apparent dispersion. The —COOD vibrations show closer agreement with experiment; nevertheless, both spectral regions can be considered well-simulated within expectations for the DFT method, which normally overestimates frequencies of C═O stretching motions. Anharmonicity of the C═O stretching potential and solvent−solute interactions not completely encompassed in the continuum solvent model[53,54] both provide sources for part of the error. The predicted C═O stretching absorption maximum intensity is larger for the —COOD than for the amide, whereas the opposite relative dipole strength is observed experimentally. This is probably due to the dispersion distributing intensity differently in the experiment (dominant

dx.doi.org/10.1021/jp502178d | J. Phys. Chem. B 2014, 118, 6937−6945

amide I band, split —COOD) and simulation (split amide I, both intense, and single —COOD) but also may be affected by the limited size of the fibril for which we could simulate spectra, since the experimental fibrils are very long.[4,36]

Overall, however, the simulations seem to provide a reasonable basis for interpreting the experimental spectra, especially for the splitting of the amide I signal into the three components and for the mode assignments. The modes calculated around the 1682 cm^{-1} band provide transition dipole moments predominantly polarized along the *x*-axis, while the 1636 and 1610 cm^{-1} bands are *y*-polarized (see also the decomposition of the spectra into the *x*, *y*, and *z* components for a randomly selected snapshot in Figure S2 (Supporting Information)). This reflects the orientation of the amide groups, more or less following the β-sheet plane.

Simulation of individual polarization components would be particularly important for oriented samples. In some experiments, the *y*-direction would correspond to the fibril growth direction, as the fibrils will predominantly lie in the plane of the sample cell window. However, without some mechanical orientation of the fibrils, it is not practical to take advantage of this internal alignment, since the *x* and *z* polarized modes would be randomly oriented. Consequently, in this study, we concentrate on the more general case of randomly oriented fibril precipitates.

The intense low frequency mode in β-sheets is *y*-polarized, and these two bands, 1636 and 1610 cm^{-1}, correspond to what is normally an intense single band, but are split here, perhaps due to our smaller structure or to edge effects in the simulated structure. The COOD modes are also predominantly polarized in the *y*- and *x*-directions, although comparatively large *z*-components occur as well, and the vibrations do not appear to be split according to the polarization.

The spectra in Figure 4 are averages of predictions for ∼190 structures obtained as snapshots from the MD runs. It is useful to ask how the spectra for the 19 annealed structures vary. There is a substantial intensity variation between them, but the basic spectral pattern and the frequencies are in fair agreement. In all, the −COOD feature at ∼1740 cm^{-1} is much more intense than other bands, but the modes associated with it all lie within a narrow range, having much less dispersion than the amide I, since it arises from only TDC coupling of the −COODs which occurs over larger distances. This lower dispersion leads to the overall high band intensity, while individual modes have similar intensities to those modes contributing to the amide I bands. The simulated amide I intensity for the snapshots is spread over four to five components, with the most intense being that at ∼1640 cm^{-1}. Most spectra have substantial bands at ∼1615 and ∼1655 cm^{-1}, although frequencies and intensities vary. Weaker bands occur at ∼1675−1685 and ∼1580−1590 cm^{-1} in some spectra. Different trajectories are qualitatively similar, but amide I intensities vary as do different snapshots in a trajectory.

The main simulated VCD features (Figure 4) are also qualitatively consistent with the experimental results for PLGA and oligomeric variants, as well as for some other fibril structures,[4] in terms of peak positions, spectral shapes, and the VCD/IR intensity ratios ($\Delta A/A = \Delta\varepsilon/\varepsilon$) if they are correlated to the computed IR absorbance spectra (thus accounting for differences in dispersion). Note that accurate determination of the fibril concentration is difficult, and thus, the experimental absorption/VCD spectra are given as dimensionless values of absorbance or differential absorbance.

The most intense experimental amide I peak in the IR corresponds to a positive "−,+" couplet. Each of the intense computed amide I features (although split) is associated with a couplet contribution of the same sign,[31] often within the broadened band shape used for comparison with experiment. As in the IR, the computed positive VCD at ∼1609 cm^{-1} does not have an experimental counterpart, perhaps due to an imperfect averaging or edge effects in the simulation. Despite the split amide I band, the overall couplet pattern in simulated VCD is qualitatively suggestive of the experimental results, with the splitting of the more intense amide I modes resulting in a more complex oscillating pattern that is exacerbated by our extensive conformational averaging.

The simulated VCD/IR ratio for the amide signal (e.g., $\Delta\varepsilon_{1633}/\varepsilon_{1636} \sim 3 \times 10^{-5}$) is much smaller than that for the PLGA experiment (e.g., $\Delta A_{1588}/A_{1600} \sim 2 \times 10^{-3}$). Such a low simulated VCD intensity is consistent with our previous DFT-based results for models of idealized structures that have no twisting in or between sheets.[19,20] Part of this difference can be explained by the flattening that modified the initial slightly twisted structure (Figure S1, Supporting Information) during the annealing in order to make the model structure better fit the periodic boundary conditions of the monoclinic box. Indeed, when we simulated the VCD spectra of the twisted alanine analogue, the $\Delta\varepsilon/\varepsilon$ ratio increased by about 10 times (see Figure S3, Supporting Information). The relative rigidity of the periodic structure is a drawback of the present model, which is otherwise well-suited to capture the compact geometry in the β_2 form of the PGA fibril, including the side chain dynamics and interactions.

As expected, VCD changes more dramatically than the absorption spectra for the different annealing cycles. In general, the net couplet nature, positive to low frequency, of the amide I VCD seen in the average VCD is detectable for each snapshot, but the shapes and positions of the bands encompass a wide variety of combinations. There is not a dominant interaction coming through in the computed spectra but rather an underlying consistent pattern that persists on the summing of many structures.

For the −COOD signal, the simulated VCD/IR intensity ratio (e.g., $\Delta\varepsilon_{1730}/\varepsilon_{1735} \sim 10^{-5}$) is again smaller than that for the PLGA experiment (e.g., $\Delta A_{1732}/A_{1729} \sim 2 \times 10^{-4}$) but has better agreement than that for the amide I. Its simulated VCD is thus relatively more intense than for experiment when compared to the amide I but is actually much weaker in absolute terms, and is composed of several overlapping alternating sign features, also as seen experimentally. This sort of pattern reflects coupling of the −COOD groups, but the detailed shape is difficult to compare to experiment due to the multiple underlying bands. The overall +/− (1752/1739 cm^{-1}) simulated couplet is negatively biased, centered around 1740 cm^{-1}, which would only approximately correspond to the dominant negative 1732 cm^{-1} PLGA experimental VCD. Note, however, that the experimental shape does vary significantly according to experimental conditions, substitution patterns in hetero-oligomers, and even the length of the poly-glutamic acid main chains. In many of these variants, this band exhibits a −/+ couplet (going to low frequency) which corresponds to the two lower components of the three-peak pattern for the experimental VCD of Glu_{10} shown in the bottom panel of Figure 4.[4,36] For our crystal model, reproducing the complete sign pattern for the solution phase fibrils might be a high goal.

dx.doi.org/10.1021/jp502178d | J. Phys. Chem. B 2014, 118, 6937−6945

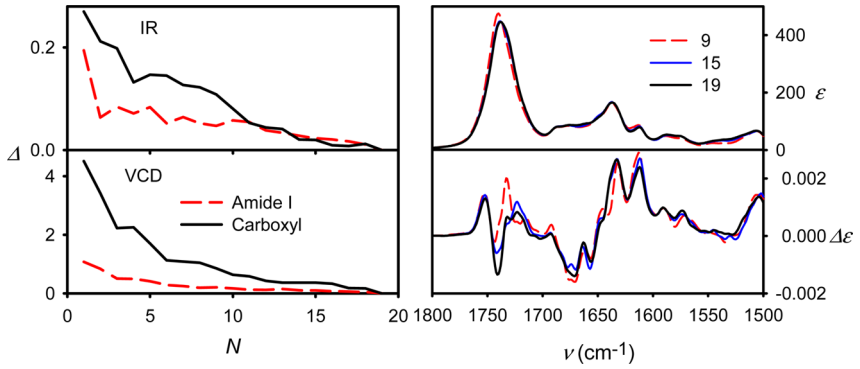

Figure 5. Absorption (top) and VCD (bottom) spectral convergence with the number of independent annealing cycles, for **y2z2**. On the left-hand side, relative integral errors ($\Delta = \int|S - S_f|\,d\nu/(\int|S|\,d\nu \int|S_f|\,d\nu)^{1/2}$, where S_f is the reference spectrum) are plotted for the carboxyl (1800−1700 cm^{-1}) and amide I (1700−1550 cm^{-1}) regions. On the right, spectra obtained by averaging of 9, 15, and 19 annealing cycles are plotted.

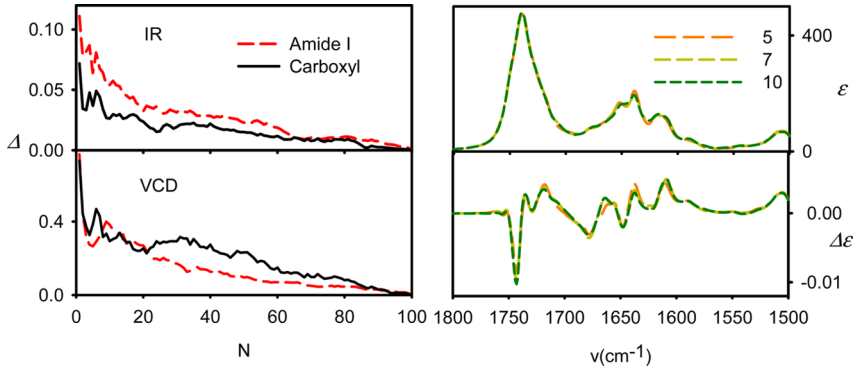

Figure 6. Absorption (top) and VCD (bottom) spectral convergence with the number of snapshots taken from a trajectory corresponding to one annealing cycle and the **y2z2** structure (as in Figure 5).

Nonetheless, the relative intensities suggest we are getting some residual local ordering of the COOD groups.

Probably the most important observation is that, in both the experiment and these MD structure-DFT computations, the −COOD band develops significant VCD even though the structures do not show an obvious systematic side-chain ordering beyond the preferred angles (Figure 3). Normally, such modes would have very little VCD due to their locally achiral structures and the low level (due to longer distance) and disordered coupling to other like modes. Certainly these oligomers and PLGA itself at higher pH have no VCD from the carboxylate, COO^-, bands (shifted below the amide I). However, the stacking of sheets constrains the side chains so that they sample a reduced configurational space, as seen in the distributions shown in Figure 3. Beyond this average distribution, the local structures presumably favor a distribution of near neighbor orientations so that the local dipolar coupling is not random. Indeed, our snapshot structures often have pairwise chiral coupling of multiple −COOD groups, which presumably do not cancel on averaging and result in a significant residual VCD.

Spectra for Fibrils of Different Sizes. The restricted size of the models used for both the fragment and extended fibril can possibly cause errors in the simulated spectral patterns. To estimate the effects of terminating the fibril in either direction (extension of H-bonds or stacking), we simulated the IR and VCD spectra for the smaller **z2**, **z4**, and **y2z2** models (as shown in Figure S4, Supporting Information) using the smaller **F8** fragment. All three structures provide similar spectral patterns, not much different from the larger **y2z3** model (Figure 4). This suggests that, as expected, the spectral shapes are mostly determined by short-range interactions between neighboring (in-strand) and direct cross-strand amide groups via covalent and dipolar interactions.

Indeed, if we compute only the spectral contributions of the inner, H-bonded amides and carboxyl groups, i.e., eliminate those from the surface groups in **y2z3** (by deleting the atomic polar and atomic axial tensors, see Figure S5, Supporting Information), this results in ∼30% loss of intensity in both the IR and VCD due to fewer oscillators contributing to the simulated spectra, but only relatively small changes occur in the correlated amide I IR and VCD patterns. However, the −COOD VCD signal changes more with respect to its absorbance. The intensity is reduced by ∼50%, and the original overall couplet is distorted to a different pattern, W-shaped (+/−/+, 1747/1735/1725 cm^{-1}). The latter shape might offer an improved agreement with experiment, but the sign is a problem and shape changes associated with this elimination of surface residues suggest that getting better agreement will require computing spectra for much larger structures, which currently is not possible for us. The loss of IR intensity is less dramatic and presumably corresponds to loss of those −COOH groups on the outside of the sheet which have no explicit acceptors for potential H-bonded interactions and are eliminated in the surface deleted computations. The variation in the VCD pattern for this mode is consistent with the experimental variations in its VCD,. as seen for glutamic acid fibrils prepared in different ways.[4,31]

The C═O vibrations in the −COOD groups most likely interact by dipolar coupling.[33] Changing the model fibril

dx.doi.org/10.1021/jp502178d | J. Phys. Chem. B 2014, 118, 6937−6945

structure to add potential interactions, i.e., between aligned sheet planes (the **z2** → **z4** elongation), and increasing the extent of cross-strand coupling in single β-sheet layers (**z2** → **y2z2**) result in relatively minor spectral changes for these side-chain modes (Figure S4, Supporting Information). That the increasing size does not increase VCD intensities or the VCD/absorption ratio (i.e., $\Delta A/A$, the g-factor) suggests that this model does not encompass the underlying interaction that leads to enhanced VCD intensity[28,55] which has been reported for some fibril structures, and is primarily seen in the amide I modes.[13] Similarly, the simulated spectra are stable with respect to the type of the dynamics: The *NpT* and *NVT* ensembles lead to very similar spectra for **y2z2** (see Figure S6, Supporting Information). In the amide I and —COOD regions, the VCD has the same overall profile after averaging over simulations for structures from both sets of trajectories, with only minor variation in detailed shapes.

Convergence of the MD Averaging. Given the partial stochastical character of the side chain conformations, stability of the simulated spectra with respect to MD parameters is of primary interest. As can be seen from Figure 5 for **y2z2** (simulated with **F8**), the absorption and VCD patterns converge with increasing number of independent annealing cycles that we sample to get initial structures for the trajectories, but VCD shows more variation, primarily in terms of spectral shapes. As expected, the −COOD IR and VCD converge more slowly than the amide I, since the side chains are more flexible. Similar convergence behavior is seen (Figure 6) with an increase in the number of snapshots averaged along a trajectory for a randomly selected annealing **y2z2** geometry, except that the amide I IR showed more variance than the −COOD IR for fewer snapshots. These MD simulations suggest that the residual VCD of the glutamic acid side chains originates in a net chiral relative orientation of the COOD groups.

Atomic Contributions to the Spectra and the TDC Model. To understand the fibrillar spectra and the relative contribution of other modes to the side-chain —COOD spectra in more detail, absorption and VCD spectra for a **y2z2** snapshot are simulated with and without contribution of the atomic intensity tensors localized on the amide (HN—C═O) atoms (Figure 7). These results show that the C═O stretching modes from both the amide and —COOD contribute almost independently to the spectra. There is only a minor contribution of the amide to the split VCD signal of —COOD at ∼1740 cm^{-1}, which is apparent as an intensity change. This suggests that interaction of the C═O transition dipoles, such as within the TDC mechanism,[50,51] is the primary source of observable VCD. For the —COOD VCD, the positive components of the "W"-like shape (the small and large maxima at 1760 and 1725 cm^{-1}) are related to predominantly y-polarized modes, whereas modes contributing to the negative lobe at 1740 cm^{-1} are x-polarized, which is consistent with the patterns seen in our larger, **y2z3** system simulation (Figure 4).

As a test of the applicability of the simpler dipole coupling (TDC) model for simulating these spectra, comparison calculations specifically for the amide and —COOD C═O stretching modes were made for the same **z2y2** structure using transition dipoles computed using *N*-methylacetamide and acetic acid as sources of the transition dipole moments, as described in the Methods section. Addition of transition dipoles corresponding to other modes, such as amide II (N—D bending and C—N stretching) and amide A (N—D stretching), changed the resultant TDC spectral pattern by less than 10%.

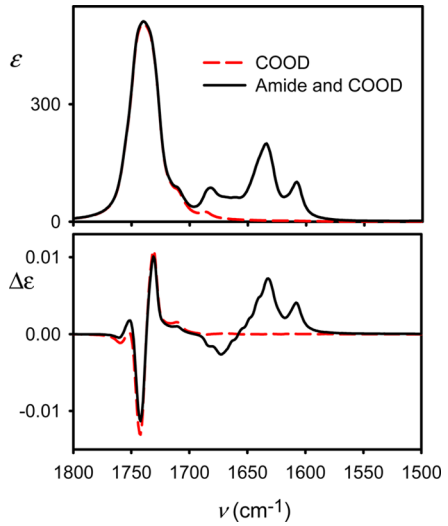

Figure 7. Absorption and VCD spectra of one **y2z2** snapshot simulated with atomic intensity tensors from just the −COOD and from both −COOD and amide groups.

One can immediately see that the TDC spectra (Figure 8) are simpler than the DFT ones (Figure 7), presumably due to the reduced set of interactions considered with the TDC method. The amide I IR is predicted as only an intense single band, while the −COOD yields a split band. Due to this change in mode dispersion, the VCD pattern that results is at least quantitatively different with the two models. The intense IR single band amide I results in an intense positive VCD couplet, which does reflect the **E10** experimental results[36] and provides only a qualitative match to the DFT results in terms of the VCD sign pattern and intensity.

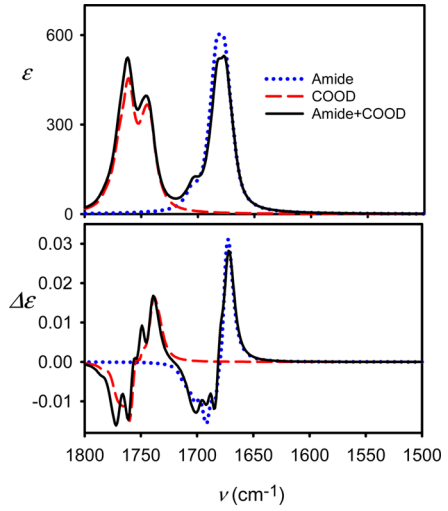

Figure 8. Absorption and VCD spectra of **y2z2** (same snapshot structure as in Figure 7) simulated using the TDC approximation, for transition dipoles on the carboxyl, the amide, and on both chromophores.

As an inherent property of the TDC mechanism, the VCD intensity is conservative (both the −COOD and amide groups give positive and negative bands of nearly the same areas). The TDC model potentially includes longer-range interactions, not

dx.doi.org/10.1021/jp502178d | J. Phys. Chem. B 2014, 118, 6937−6945

present in the DFT computations due to the transfer of parameters from limited size fragments, but these long-range couplings do not have a large effect, although they might explain the −COOD IR band splitting, reproduced only partially by DFT (cf. the discussion of Figure 4). The $\Delta\varepsilon/\varepsilon$ ratio obtained by TDC is about the same as that for DFT, probably because of the neglect of the fibril twist in both models. The −COOD VCD intensity in Figures 7 and 8 is enhanced, since these are single snapshots without averaging. Averaging over many snapshots causes more cancellation in the side-chain modes due their increased variation in conformation.

We can summarize what was learned from the modeling of poly-glutamic acid side chain VCD: It originates in a partial chiral orientation of the −COOD groups on the side chains and their dipole−dipole interaction. It is fairly uncoupled to the amide and other peptide vibrational modes, and is polarized within the side chain layer sandwiched between the β-sheet planes. Using these insights, the VCD of this or other side chains can possibly be used to probe the geometry of the intersheet space as well as to complement the information about fibril structure obtained from the amide I modes.

CONCLUSIONS

In order to explain the VCD spectra observed for the side chains of the poly-glutamic acid, which has been shown to form dense β_2 fibrils, we adopted a crystal-like geometry model. With several annealing cycles and a molecular dynamic equilibration, we verified that the structure was stable both at the *NVT* and *NpT* conditions. The angular distribution thus obtained confirmed the side chains maintained a limited local ordering, although not a periodic or crystalline structure. Using the Cartesian coordinate-based transfer of the force field and intensity tensors calculated for smaller fragments, absorption and VCD spectra of larger stacked sheet segments could be simulated that showed qualitative features in common with experimental data on Glu_{10} (**E10**) fibrillar systems. These simulations gave IR spectral patterns in reasonable agreement with experiment, although edge effects seem to distort the dispersion. We were not able to replicate the VCD enhancement seen experimentally for the amide I mode in fibrils. In spite of the statistical character, the averaged spectral patterns converged relatively quickly with the number of MD snapshots and annealing cycles. Analysis of the calculated side-chain VCD indicated that it reflects a residual chiral mutual −COOH group coupling, developed through population of a few favored conformations, but evidences only limited interaction with the amide group. VCD spectroscopy combined with the simulations is thus able to recognize very specific geometry features of fibrillar structures.

ASSOCIATED CONTENT

Supporting Information

Computational details and various computational tests. This material is available free of charge via the Internet at http://pubs.acs.org.

AUTHOR INFORMATION

Corresponding Authors

*E-mail: tak@uic.edu.

*E-mail: bour@uochb.cas.cz.

Notes

The authors declare no competing financial interest.

ACKNOWLEDGMENTS

The work was supported by the Academy of Sciences (M200550902), Grant Agency of the Czech Republic (P208/11/0105), and Ministry of Education (LH11033, LM2010005, CZ.1.05/3.2.00/08.0144). The work was done in part while T.A.K. was a guest Professor at the University of Konstanz supported as a Research Awardee of the Alexander von Humboldt Foundation.

REFERENCES

(1) Harrison, P. M.; Bamborough, P.; Daggett, V.; Prusiner, S. B.; Cohen, F. E. The Prion Folding Problem. *Curr. Opin. Struct. Biol.* **1997**, *7*, 53−59.

(2) Miranker, A. D.; Dobson, C. M. Collapse and Cooperativity in Protein Folding. *Curr. Opin. Struct. Biol.* **1996**, *6*, 31−42.

(3) Morris, K. L.; Serpell, L. C. X-Ray Fibre Diffraction Studies of Amyloid Fibrils. *Methods Mol. Biol.* **2012**, *849*, 121−135.

(4) Fulara, A.; Lakhani, A.; Wójcik, S.; Nieznańska, H.; Keiderling, T. A.; Dzwolak, W. Spiral Superstructures of Amyloid-Like Fibrils of Polyglutamic Acid: An Infrared Absorption and Vibrational Circular Dichroism Study. *J. Phys. Chem. B* **2011**, *115*, 11010−11016.

(5) Benditt, E. P.; Eriksen, N.; Berglund, C. Congo Red Dichroism with Dispersed Amyloid Fibrils, an Extrinsic Cotton Effect. *Proc. Natl. Acad. Sci. U.S.A* **1970**, *66*, 1044−1051.

(6) Yamamoto, S.; Watarai, H. Raman Optical Activity Study on Insulin Amyloid and Prefibril Intermediate. *Chirality* **2012**, *24*, 97−103.

(7) Reichert, D.; Pascui, O.; deAzevedo, E. R.; Bonagamba, T. J.; Arnold, K.; Huster, D. A Solid-State NMR Study of the Fast and Slow Dynamics of Collagen Fibrils at Varying Hydration Levels. *Magn. Reson. Chem.* **2004**, *42*, 276−284.

(8) Kanaori, K.; Nosaka, A. Y. Characterization of Human Calcitonin Fibrillation in Aqueous Urea Solution by H-1 NMR Spectroscopy. *Biochemistry* **1996**, *35*, 12671−12676.

(9) Dzwolak, W.; Loksztejn, A.; Galinska-Rakoczy, A.; Adachi, R.; Goto, Y.; Rupnicki, L. Conformational Indeterminism in Protein Misfolding: Chiral Amplification on Amyloidogenic Pathway of Insulin. *J. Am. Chem. Soc.* **2007**, *129*, 7517−7522.

(10) Maa, S.; Cao, X.; Mak, M.; Sadik, A.; Walkner, C.; Freedman, T. B.; Lednev, I.; Dukor, R.; Nafie, L. Vibrational Circular Dichroism Shows Unusual Sensitivity to Protein Fibril Formation and Development in Solution. *J. Am. Chem. Soc.* **2007**, *129*, 12364−12365.

(11) Kurouski, D.; Lombardi, R. A.; Dukor, R. K.; Lednev, I. K.; Nafie, L. A. Direct Observation and pH Control of Reversed Supramolecular Chirality in Insulin Fibrils by Vibrational Circular Dichroism. *Chem. Commun.* **2010**, *46*, 7154−7156.

(12) Kurouski, D.; Dukor, R. K.; Lu, X.; Nafie, L. A.; Lednev, I. K. Spontaneous Inter-Conversion of Insulin Fibril Chirality. *Chem. Commun.* **2012**, *48*, 2837−2839.

(13) Kurouski, D.; Kar, K.; Wetzel, R.; Dukor, R. K.; Lednev, I. K.; Nafie, L. A. Levels of Supramolecular Chirality of Polyglutamine Aggregates Revealed by Vibrational Circular Dichroism. *FEBS Lett.* **2013**, *578*, 1638−1643.

(14) Nishijima, M.; Tanaka, H.; Yang, C.; Fukuhara, G.; Mori, T.; Babenko, V.; Dzwolak, W.; Inoue, Y. Supramolecular Photochirogenesis with Functional Amyloid Superstructures. *Chem. Commun.* **2013**, *49*, 8916−8918.

(15) Babenko, V.; Piejko, M.; Wójcik, S.; Mak, P.; Dzwolak, W. Vortex-Induced Amyloid Superstructures of Insulin and its Component A and B Chains. *Langmuir* **2013**, *29*, 5271−5278.

(16) Babenko, V.; Dzwolak, W. Amino Acid Sequence Determinants in Self-Assembly of Insulin Chiral Amyloid Superstructures: Role of C-Terminus of B-Chain in Association of Fibrils. *FEBS Lett.* **2013**, *587*, 625−630.

(17) Dzwolak, W.; Surmacz-Chwedoruk, W.; Babenko, V. Conformational Memory Effect Reverses Chirality of Vortex-Induced Insulin Amyloid Superstructures. *Langmuir* **2013**, *29*, 365−370.

(18) Wójcik, S.; Babenko, V.; Dzwolak, W. Insulin Amyloid Superstructures as Templates for Surface Enhanced Raman Scattering. *Langmuir* **2010**, *26*, 18303−18307.
(19) Welch, W. R. W.; Keiderling, T. A.; Kubelka, J. Structural Analyses of Experimental 13c Edited Amide I′ IR and VCD for Peptide β-Sheet Aggregates and Fibrils Using DFT-Based Spectral Simulations. *J. Phys. Chem. B* **2013**, *117*, 10359−10369.
(20) Welch, W. R. W.; Kubelka, J.; Keiderling, T. A. Infrared, Vibrational Circular Dichroism, and Raman Spectral Simulations for β-Sheet Structures with Various Isotopic Labels, Interstrand, and Stacking Arrangements Using Density Functional Theory. *J. Phys. Chem. B* **2013**, *117*, 10343−10358.
(21) Measey, T.; Schweitzer-Stenner, R. Vibrational Circular Dichroism as a Probe of Fibrillogenesis: The Origin of the Anomalous Intensity Enhancement of Amyloid-Like Fibrils. *J. Am. Chem. Soc.* **2011**, *133*, 1066−1076.
(22) Karjalainen, E. L.; Ravi, H. K.; Barth, A. Simulation of the Amide I Absorption of Stacked β-Sheets. *J. Phys. Chem. B* **2011**, *115*, 749−757.
(23) Mandal, P.; Eremina, N.; Barth, A. Formation of Two Different Types of Oligomers in the Early Phase of pH-Induced Aggregation of the Alzheimer Aβ(12−28) Peptide. *J. Phys. Chem. B* **2012**, *116*, 12389−12397.
(24) Bouř, P.; Sopková, J.; Bednárová, L.; Maloň, P.; Keiderling, T. A. Transfer of Molecular Property Tensors in Cartesian Coordinates: A New Algorithm for Simulation of Vibrational Spectra. *J. Comput. Chem.* **1997**, *18*, 646−659.
(25) Yamamoto, S.; Li, X.; Ruud, K.; Bouř, P. Transferability of Various Molecular Property Tensors in Vibrational Spectroscopy. *J. Chem. Theory Comput.* **2012**, *8*, 977−985.
(26) Bieler, N. S.; Haag, M. P.; Jacob, C. R.; Reiher, M. Analysis of the Cartesian Tensor Transfer Method for Calculating Vibrational Spectra of Polypeptides. *J. Chem. Theory Comput.* **2011**, *7*, 1867−1881.
(27) Bouř, P.; Keiderling, T. A. Ab Initio Simulation of the Vibrational Circular Dichroism of Coupled Peptides. *J. Am. Chem. Soc.* **1993**, *115*, 9602−9607.
(28) Andrushchenko, V.; Bouř, P. Circular Dichroism Enhancement in Large DNA Aggregates Simulated by a Generalized Oscillator Model. *J. Comput. Chem.* **2008**, *29*, 2693−2703.
(29) Bak, K. L.; Jorgensen, P.; Helgaker, T.; Ruud, K. Basis Set Convergence and Correlation Effects in Vibrational Circular Dichroism Calculations Using London Orbitals. *Faraday Discuss.* **1994**, *99*, 121−129.
(30) Cheeseman, J. R.; Frisch, M. J.; Devlin, F. J.; Stephens, P. J. Ab Initio Calculation of Atomic Axial Tensors and Vibrational Rotational Strengths Using Density Functional Theory. *Chem. Phys. Lett.* **1996**, *252*, 211−220.
(31) Setnička, V.; Huang, R.; Thomas, C. L.; Etienne, M. A.; Kubelka, J.; Hammer, R. P.; Keiderling, T. A. IR Study of Cross-Strand Coupling in a Beta-Hairpin Peptide Using Isotopic Labels. *J. Am. Chem. Soc.* **2005**, *127*, 4992−4993.
(32) Huang, R.; Setnička, V.; Etienne, M. A.; Kim, J.; Kubelka, J.; Hammer, R. P.; Keiderling, T. A. Cross-Strand Coupling of a β-Hairpin Peptide Stabilized with an Aib-Gly Turn Using Isotope-Edited IR Spectroscopy. *J. Am. Chem. Soc.* **2007**, *129*, 13592−13603.
(33) Kubelka, J.; Kim, J.; Bouř, P.; Keiderling, T. A. Contribution of Transition Dipole Coupling to Amide Coupling in IR Spectra of Peptide Secondary Structures. *Vib. Spectrosc.* **2006**, *42*, 63−73.
(34) Keith, H. D.; Giannoni, G.; Padden, F. J. Single Crystal of Poly(L-Glutamic Acid). *Biopolymers* **1969**, *7*, 775−792.
(35) Itoh, K.; Foxman, B. M.; Fasman, G. D. The Two β-Forms of Poly(L-Glutamic Acid). *Biopolymers* **1976**, *15*, 419−455.
(36) Chi, H.; Welch, W. R. W.; Kubelka, J.; Keiderling, T. A. Insight into the Packing Pattern of β2 Fibrils: A Model Study of Glutamic Acid Rich Oligomers with 13-C Isotopic Edited Vibrational Spectroscopy. *Biomacromolecules* **2013**, *14*, 3880−3891.
(37) Pronk, S.; Páll, S.; Schulz, R.; Larsson, P.; Bjelkmar, P.; Apostolov, R.; Shirts, M. R.; Smith, J. C.; Kasson, P. M.; vanderSpoel, D.; et al. Gromacs 4.5: A High-Throughput and Highly Parallel Open Source Molecular Simulation Toolkit. *Bioinformatics* **2013**, *27*, 845−854.
(38) Kamiya, N.; Watanabe, Y. S.; Ono, S.; Higo, J. Amber-Based Hybrid Force Field for Conformational Sampling of Polypeptides. *Chem. Phys. Lett.* **2005**, *401*, 312−317.
(39) Bouř, P.; Keiderling, T. A. Partial Optimization of Molecular Geometry in Normal Coordinates and Use as a Tool for Simulation of Vibrational Spectra. *J. Chem. Phys.* **2002**, *117*, 4126−4132.
(40) Bouř, P. Convergence Properties of the Normal Mode Optimization and its Combination with Molecular Geometry Constraints. *Collect. Czech. Chem. Commun.* **2005**, *70*, 1315−1340.
(41) Hudecová, J.; Hopmann, K. H.; Bouř, P. Correction of Vibrational Broadening in Molecular Dynamics Clusters with the Normal Mode Optimization Method. *J. Phys. Chem. B* **2012**, *116*, 336−342.
(42) Frisch, M. J.; Trucks, G. W.; Schlegel, H. B.; Scuseria, G. E.; Robb, M. A.; Cheeseman, J. R.; Scalmani, G.; Barone, V.; Mennucci, B.; Petersson, G. A.; et al. *Gaussian 09*, revision B01; Gaussian, Inc.: Wallingford, CT, 2009.
(43) Becke, A. Density-Functional Exchange-Energy Approximation with Correct Asymptotic Behavior. *Phys. Rev. A* **1988**, *38*, 3098−3100.
(44) Klamt, A. Cosmo and Cosmo-Rs. In *The Encyclopedia of Computational Chemistry*; Schleyer, P. R., Allinger, N. L., Clark, T., Gasteiger, J., Kollman, P. A., Schaefer, H. F., III, Schreiner, P. R., Eds.; John Wiley & Sons: Chichester, U.K., 1998; Vol. *1*, pp 604−615.
(45) Hudecová, J.; Profant, V.; Novotná, P.; Baumruk, V.; Urbanová, M.; Bouř, P. Ch Stretching Region: Computational Modeling of Vibrational Optical Activity. *J. Chem. Theory Comput.* **2013**, *9*, 3096−3108.
(46) Nafie, L. *Vibrational Optical Activity: Principles and Applications*; Wiley: Chichester, U.K., 2011.
(47) Holzwarth, G.; Chabay, I. Optical Activity of Vibrational Transitions: A Coupled Oscillator Model. *J. Chem. Phys.* **1972**, *57*, 1632−1635.
(48) Zhong, W.; Gulotta, M.; Goss, D. J.; Diem, M. DNA Solution Conformation Via Infrared Circular Dichroism: Experimental and Theoretical Results for B-Family Polymers. *Biochemistry* **1990**, *29*, 7485−7491.
(49) Yamaoki, Y.; Imamura, H.; Fulara, A.; Wójcik, S.; Bożycki, Ł.; Kato, M.; Keiderling, T. A.; Dzwolak, W. An FT-IR Study on Packing Defects in Mixed β-Aggregates of Poly(L-glutamic Acid) and Poly(D-Glutamic Acid): A High-Pressure Rescue from a Kinetic Trap. *J. Phys. Chem. B* **2012**, *116*, 5172−5178.
(50) Rick, S. W.; Cachau, R. E. The Nonplanarity of the Peptide Group: Molecular Dynamics Simulations with a Polarizable Two-State Model for the Peptide Bond. *J. Chem. Phys.* **2000**, *112*, 5230−5241.
(51) Andrushchenko, V.; Matějka, P.; Anderson, D. T.; Kaminský, J.; Horníček, J.; Paulson, L. O.; Bouř, P. Solvent Dependence of the N-Methylacetamide Structure and Force Field. *J. Phys. Chem. A* **2009**, *113*, 9727−9736.
(52) Creighton, T. E. *Proteins: Structures and Molecular Properties*, 2nd ed.; W. H. Freeman and Co.: New York, 1993.
(53) Kubelka, J.; Keiderling, T. A. Ab Initio Calculation of Amide Carbonyl Stretch Vibrational Frequencies in Solution with Modified Basis Sets. 1. N-Methyl Acetamide. *J. Phys. Chem. A* **2001**, *105*, 10922−10928.
(54) Bouř, P. On the Influence of the Water Electrostatic Field on the Amide Group Vibrational Frequencies. *J. Chem. Phys.* **2004**, *121*, 7545−7548.
(55) Profant, V.; Baumruk, V.; Li, X.; Šafařík, M.; Bouř, P. Tracking of the Polyproline Folding by Density Functional Computations and Raman Optical Activity Spectra. *J. Phys. Chem. B* **2011**, *115*, 15079−11589.